Available online at www.sciencedirect.com
ScienceDirect
Trans. Nonferrous Met. Soc. China 28(2018) 739−747
Transactions of Nonferrous Metals Society of China
www.tnmsc.cn

Influence of La precursors on structure and properties of CeO_2−ZrO_2−Al_2O_3 composite oxides

You-feng LI[1], Yue-hui HE[2], Guo-qing LIU[1], Ling-wei ZENG[1]

1. School of Chemistry and Chemical Engineering,
Hunan University of Science and Technology, Xiangtan 411201, China;
2. Research Institute of Powder Metallurgy, Central South University, Changsha 410083, China

Received 19 October 2016; accepted 4 November 2017

Abstract: Three La-doped CeO_2−ZrO_2−Al_2O_3 (CZA) composite oxide samples, namely, CZA-I, CZA-II and CZA-III, were prepared following a co-precipitation method in the presence of La_2O_3, $La(NO_3)_3{\cdot}6H_2O$ and $H[La(EDTA)]{\cdot}16H_2O$ precursors, respectively. When the precursor samples are sintered at 1000 °C, the as-prepared composite oxides mainly exhibit the CeO_2−ZrO_2 cubic fluorite phase, while the γ-Al_2O_3 and δ-Al_2O_3 phases appear when the precursor samples are subjected to sintering at 1100 and 1200 °C. CZA-III exhibits improved redox properties after high-temperature treatment compared with CZA-I and CZA-II. CZA-III presents the largest surface area of 97.46 m^2/g among the three CZAs when the CZA-III precursor sample is sintered at 1000 °C. Furthermore, the corresponding oxygen storage capacity (OSC) is the largest with value of 400.27 μmol/g when CZA-III precursor sample is sintered at 1000 °C. Additionally, CZA-III exhibits the best thermal stability and the highest reduction temperature. However, by increasing the sintering temperature to 1200 °C, there is a dramatic decline in the properties of surface area and OSC. And a decrease for CZA-III in surface area by 58.94% and a decrease of the OSC value by 74.56% are observed.
Key words: La precursor; ceria−zirconia solid solution; composite oxide; texture structure; redox property

1 Introduction

Automobile emissions containing CO, hydrocarbons, nitrogen oxides, sulfur dioxide and other waste gases are an environmental concern as they are major air pollutants. Three-way catalysts, which mainly comprise the carrier and Pt, Pd or Rh noble metal active components, can simultaneously eliminate these contaminated waste gases. Ceria-based oxides have been extensively used as the carrier on the merit of their oxygen storage capability via the reaction $2CeO_2 \leftrightarrow Ce_2O_3+1/2O_2$ [1−4]. However, pure CeO_2 is easily susceptible to sintering at 800 °C, resulting in a reduction in surface area and oxygen storage capacity (OSC) [5]. It has been reported that $Ce_xZr_{1-x}O_2$ generated by doping ZrO_2 into CeO_2, can significantly improve the stability of ceria against high temperature sintering and thus inhibit the decrease of OSC [6−8]. As known, γ-Al_2O_3 is commonly used as a gas purification catalyst carrier because of the nature of its porous structure and high specific surface area. MONTE et al [9] successfully inserted Al_2O_3 into $Ce_xZr_{1-x}O_2$ to improve the specific surface area and OSC of the composite oxide. However, in previous studies [10,11], significant reductions to specific surface area were observed as a result of particle sintering, pore collapse and γ-Al_2O_3 phase transition when subjecting the materials to high temperature of 1000 °C. Therefore, the thermal stability of the $Ce_xZr_{1-x}O_2$ composite oxides is still an important issue when the operation temperature of the catalysts exceeds 1000 °C. Incorporation of other rare earth ions to $Ce_xZr_{1-x}O_2$ can further enhance the thermal stability. SI et al [12] observed that surface area and thermal stability were enhanced by doping Y, La, or Pr into $Ce_xZr_{1-x}O_2$. MENG and JI [13] studied the influence of La_2O_3 particle size on the oxidation resistance of electrodeposited Ni−La_2O_3/CeO_2 composites at 1000 °C. WANG et al [14] discovered that catalyst-supported materials of tetragonal ZrO_2 were stabilized by La_2O_3 and possessed well-defined shape and size, and superior thermal stability (up to 1000 °C). According to the results of BOZO

Foundation item: Project (14JJ4043) supported by the Natural Science Foundation of Hunan Province, China
Corresponding author: You-feng LI; Tel: +86-731-58290045; E-mail: liyoufeng2005@sina.com
DOI: 10.1016/S1003-6326(18)64706-5

et al [15], incorporation of some rare earth ions can significantly increase the number of oxygen vacancies in $Ce_xZr_{1-x}O_2$ and improve oxygen activation. The doped composites normally possess significantly more crystal defects and maintain a relatively high surface area after calcination. Usually, these rare earth ions are introduced into the reaction system via their corresponding nitrate precursors. There are few reports related to the influence of varying the rare earth ion precursors and addition methods on the structure and properties of $Ce_xZr_{1-x}O_2$.

In the present work, La rare earth ions were introduced into CeO_2−ZrO_2−Al_2O_3 (CZA) composites via La_2O_3, $La(NO_3)_3·6H_2O$ and $H[La(EDTA)]·16H_2O$ precursors, yielding three composite oxide samples, CZA-I, CZA-II and CZA-III, respectively. The influence of the La precursors on the crystal phase, thermal stability, structural and textural properties, OSC and temperature-programmed reduction (TPR) properties of the three composite oxides was investigated systematically. Finally, CZA composite oxides doped with La were studied to increase their thermal stabilities and redox properties.

2 Experimental

2.1 Preparation of La-doped composite oxides

Fresh CZA composite oxides were prepared following a co-precipitation method. The nitrate precursors of $Ce(NO_3)_3·6H_2O$, $Zr(NO_3)_4·5H_2O$ and $Al(NO_3)_3·9H_2O$ were employed as reactive materials. La rare earth ions were introduced via the addition of La_2O_3, $La(NO_3)_3·6H_2O$ and $H[La(EDTA)]·16H_2O$ precursors, respectively. The molar ratio of Ce:Zr:Al was controlled at 1:1:5, and the theoretical mole fraction of La was 2%. Polyethylene glycol (PEG) as the dispersant and $NH_4HCO_3NH_3·H_2O$ as the precipitator were added into the mixture to aid precipitation at 80 °C under agitation. After being aged at room temperature for 24 h, the precipitate was filtrated and washed with deionized water. The loose precursor samples were obtained after the precipitates were dried at 100 °C for 10 h, followed by calcination in a muffle furnace at 300 °C for 6 h. The CZA samples were prepared by sintering the as-obtained loose precursors at 1000, 1100 and 1200 °C for 4 h. The corresponding CZA samples deriving from the La_2O_3, $La(NO_3)_3·6H_2O$ and $H[La(EDTA)]·16H_2O$ precursors were denoted as CZA-I, CZA-II and CZA-III, respectively. The CZA samples were employed as the reference samples to demonstrate the influence of different La precursors on the structure and properties of the composite oxides.

2.2 Material characterization

The crystalline phases of the as-prepared composite oxides were studied by X-ray diffraction (XRD) using a Bruker/AXS D8 Advance X-ray diffractometer operated at 40 kV and 200 mA with Cu K_α radiation (λ=0.15418 nm). Thermogravimetric analysis (TGA) was conducted in a nitrogen flow of 60 mL/min at a rate of 5 °C/min on an STD Q600 instrument. The morphology and dispersion of the powders were observed using a scanning electron microscope (SEM, JEOL−6360LV). Textural properties of the samples were measured by the Brunauer−Emmett−Teller (BET) model with a Quantachrome NOVA instrument using Ar as the carrier gas and N_2 as the adsorbent. Total OSC was measured via the oxygen pulse method. H_2-temperature programmed reduction (H_2-TPR) experiments were performed in a conventional system equipped with a thermal conductivity detector.

3 Results and discussion

3.1 Crystal structure analysis

The XRD results of the CZA samples obtained from different La precursors, as a function of sintering temperature, are shown in Fig. 1. Clear diffraction peaks are observed at 2θ of ~28.5°, ~33.0°, ~47.5°, ~59.0°, ~69.5° and 79.0°, in agreement with the (111), (200), (220), (311), (400) and (422) planes of the cubic fluorite structure of CeO_2, respectively. Some weak peaks of γ-Al_2O_3 are also observed on the XRD patterns for the samples sintered at 1100 °C. However, the peak intensity for γ-Al_2O_3 and δ-Al_2O_3 phases significantly increases when subjecting the samples to sintering temperature of 1200 °C. XRD results show that ceria−zirconia solid solutions form. Additionally, the γ-Al_2O_3 phase arises at 1100 °C because of the instability and sintering phenomenon of the ceria−zirconia solid solutions. The γ-Al_2O_3 phase transforms to the δ-Al_2O_3 phase at 1200 °C. The La in the samples is not detected by XRD, indicating that La^{3+} cations have been well inserted into the CeO_2−ZrO_2 lattice, or amorphous La_2O_3-based clusters are well dispersed on the surface of the CeO_2−ZrO_2 matrix and Al_2O_3 particles [16]. As the sintering temperature increases, there is a reduction in full width at half maximum of the diffraction peaks together with an increase in the diffraction peak intensity, indicating improved crystallization and larger crystal sizes with increasing temperature. The above trend is the most obvious for CZA-III doped with the H[La(EDTA)] precursor; however, the trend is not observed for CZA-II doped with the $La(NO_3)_3$ precursor. CZA-III has the lowest degree of crystallization at 1000 °C but displays the highest degree of crystallinity when being subjected to a sintering temperature of 1200 °C. It is noticed that the diffraction peaks of CZA-I sintered at 1200 °C are slightly shifted to lower diffraction angles, which can be

attributed to lattice shrinkage because of the replacement of Ce^{4+} cations with La^{3+} cations. The substitution of the small-sized Ce^{4+} (r=0.097 nm) with La^{3+} (r=0.120 nm) results in an increase in lattice dimensions, thereby the diffraction peaks shifting to lower diffraction angles [17].

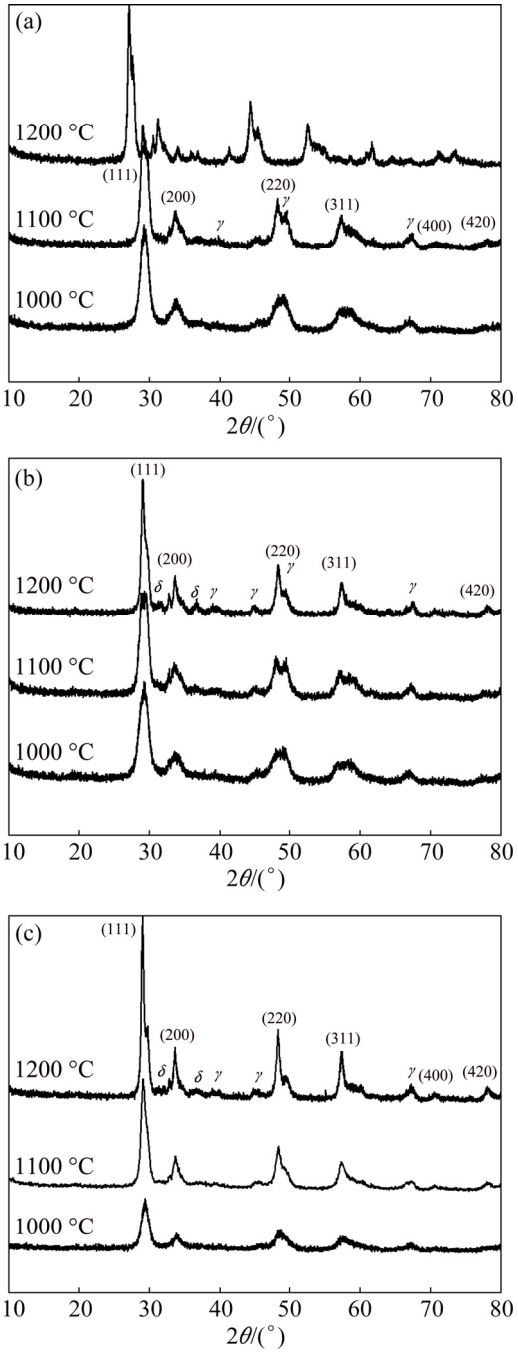

Fig. 1 X-ray diffraction patterns of different CeO_2−ZrO_2−Al_2O_3 (CZA) composite oxides: (a) CZA-I; (b) CZA-II; (c) CZA-III

This exchange results as the interactions between La and the CZA matrix material differ with various La precursors. With the addition of La_2O_3 into the matrix, CZA-I sample has the weakest interaction force, and free La_2O_3 can be distributed on the surface of the CeO_2−ZrO_2 matrix and Al_2O_3 particles. Since there is a preference for La^{3+} to replace Ce^{4+} at 1200 °C, there is a crystal lattice blue-shift phenomenon. $La(NO_3)_3$ has been employed as a precursor in precipitation reactions as other nitrates, when $La(NO_3)_3$ is added into the reaction system. The La^{3+} cations have been incorporated into the CeO_2−ZrO_2 lattice and thereafter solid solutions form. There are cases in which the $La(NO_3)_3$ precursor has little effect on the crystal structure during heat treatment process. There is a stable complex in the presence of H[La(EDTA)]. In this case, the CZA-III matrix exhibits the highest thermal stability for the five-membered rings composed of metals cations and EDTA [18]. Hence, crystallization of the samples is the lowest at 1000 °C among all products, and the product crystallinity is the highest when subjecting the EDTA-containing matrix to combustion at 1200 °C.

3.2 Thermal stability analysis

Figure 2 shows the thermogravimetric analysis (TGA)/differential scanning calorimetry (DSC) curves of the dried CZA precipitate at a heating rate of 5 °C/min. DSC curves display endothermic peaks and exothermic peaks. The endothermic peaks at ~150 °C can be explained by the removal of adsorbed water and crystal water. The exothermic peaks at ~200 °C can be attributed to the burning and decomposition of PEG in the precipitate precursors. Major mass loss of the precipitate precursors occurs at ~400 °C. The overall mass loss is approximately 80%. The exothermic peaks of CZA-I, in the presence of the La_2O_3 additive, at 590 and 735 °C can be attributed to crystallization and crystal growth of CeO_2−ZrO_2 and γ-Al_2O_3 matrix, respectively. At ~1110 °C, there is another exothermic peak that shows γ-Al_2O_3 phase transition. The exothermic peaks of CZA-II, containing the $La(NO_3)_3$ additive, at 605 °C, are also ascribed to the crystallization and crystal growth of CeO_2−ZrO_2 and γ-Al_2O_3 matrix. There are no other changes in the TGA/DSC curves above 750 °C, suggesting that the precursor powders have been completely transformed to the CeO_2−ZrO_2 cubic crystal phase and the γ-Al_2O_3 matrix phase, as confirmed by the XRD results in Fig. 1(b). An exothermic peak occurs for the H[La(EDTA)] additive sample during the heating process at ~960 °C, which implies the formation of the CeO_2−ZrO_2 and γ-Al_2O_3 crystal phases. This is consistent with the XRD results in Fig. 1(c). It is obvious that the diffraction peaks of CZA-III are weak at 1000 °C; however, the XRD peak intensity of CZA-III is the strongest among all the samples sintered at 1200 °C when the EDTA complex decomposes and releases heat. Mass loss of the CZA-III sample can also be observed above 1000 °C (Fig. 2(c)).

Figures 1 and 2 indicate that varying La precursors directly influence the thermal stability and crystal

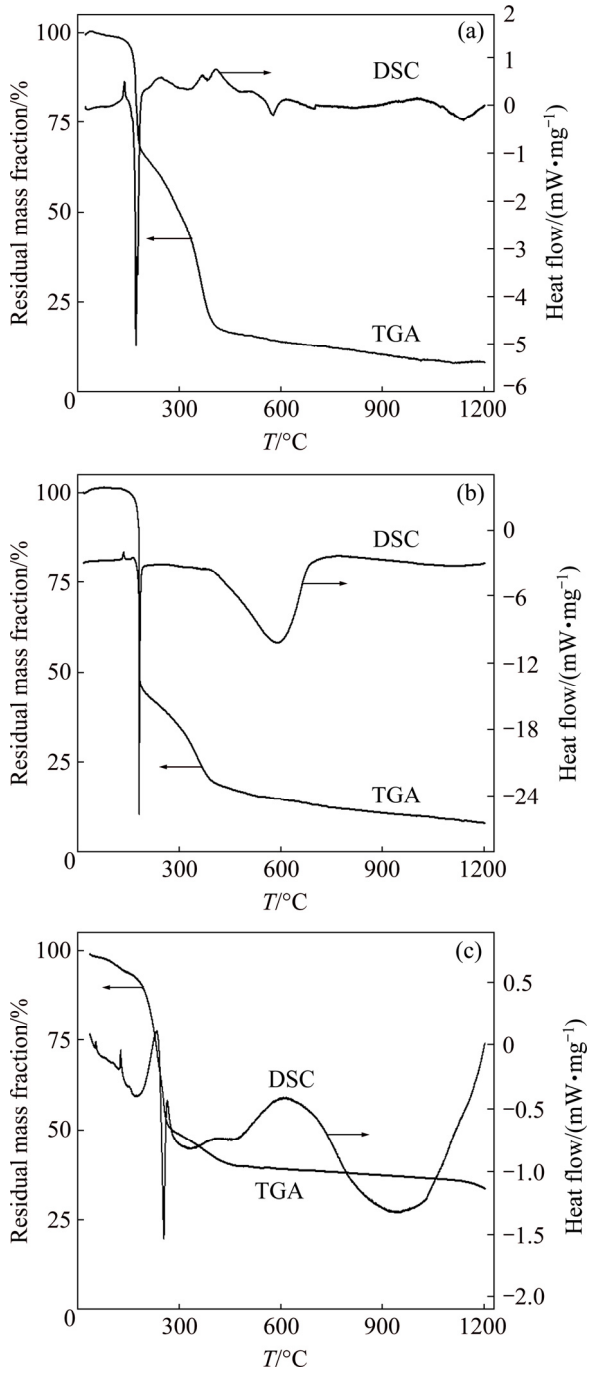

Fig. 2 Thermogravimetric analysis (TGA)/differential scanning calorimetry (DSC) curves of CZA precipitate precursors: (a) CZA-I; (b) CZA-II; (c) CZA-III

structure of the CZA composites, which can be attributed to the nature of the interaction between the CZA matrix and the La_2O_3, $La(NO_3)_3{\cdot}6H_2O$ or $H[La(EDTA)]{\cdot}16H_2O$ precursors. When EDTA is added into the reaction solution, a stable complex is generated and the corresponding samples demonstrate higher degrees of stability. When $La(NO_3)_3{\cdot}6H_2O$ precursor is added into the solution, it takes part in the co-precipitation reaction as other nitrate materials. The corresponding precursor completely transforms into the CeO_2–ZrO_2 cubic crystal phase and γ-Al_2O_3 phase at ~605 °C. However, when La_2O_3 is added into the reaction solution, this La_2O_3 precursor does not undergo any reaction until ~1110 °C and replaces the Ce^{4+} cations. There is obvious agreement between the XRD results and the thermal analysis results.

3.3 Product morphology analysis

Figure 3 shows the SEM images of the CZA samples sintered at 1000 °C and 1200 °C for 4 h. There are some differences in morphology of the CZA samples depending on the precursors employed. In the presence of La_2O_3, the crystals display a fibrous porous nature, while the products are porous and granular when the $La(NO_3)_3{\cdot}6H_2O$ additive is used. A porous spongy texture is observed for the samples synthesized using the $H[La(EDTA)]{\cdot}16H_2O$ precursor. It is clear that both particle size and pore size increase as a function of increased sintering temperature. The interstitial pore size among particles is ~15 nm at 1000 °C, which increases to ~40 nm at 1200 °C. The increase of particle size and pore size leads to a significant decrease of the BET surface area. Furthermore, varying the precursors directly influences CZA product morphologies, textural properties and oxygen storage capacities.

Generally, the morphology of the CZA product is closely related to its growth surroundings [19,20]. The surroundings can be controlled through chemical bonding, sintering temperature and sintering time. There are small differences in structure for a low doping content of La and the same doping content of the PEG dispersant at the same sintering temperature. The particles grow and become coarse as the sintering temperature increases. The interstitial pores grow accordingly when the precursor samples are sintered at 1200 °C. So, the morphology and pore structure of CZA composite oxides vary under different conditions.

3.4 Texture structure and oxygen storage capacity analysis

Textural properties of the samples were investigated by N_2 adsorption and desorption isotherms. Figure 4 displays the pore diameter distribution of CZA-I, CZA-II and CZA-III sintered at 1000 and 1200 °C. The mean pore diameters (d_p) of the samples are ~15 and ~40 nm after the precursor are samples sintered at 1000 and 1200 °C, respectively. The pore diameter and the pore volume display normal distributions. The mean pore size of the sample in the presence of the $La(NO_3)_3$ precursor is smaller, while using to the EDTA and La_2O_3 precursors sintered at 1200 °C results in an increase in the mean pore size. The EDTA and La_2O_3 precursors in the materials obviously show a shift to larger pore size; hence, the anti-aging properties of the corresponding

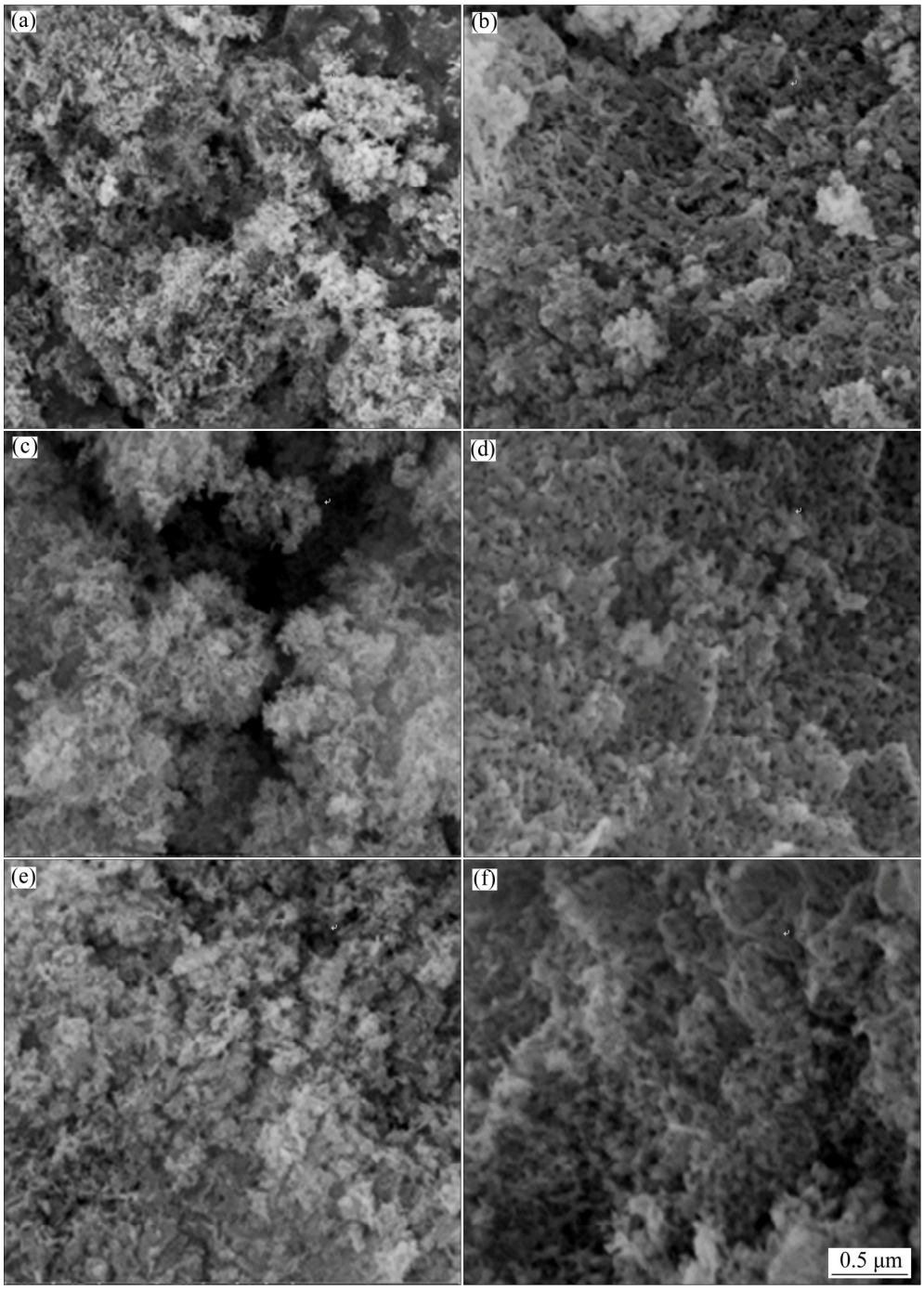

Fig. 3 Scanning electron microscopy images of CZA samples doped with different La precursors after sintering at 1000 °C (a, c, e) and 1200 °C (b, d, f): (a, b) CZA-I; (c, d) CZA-II; (e, f) CZA-III

products are enhanced. However, the pore volume (V) is smaller for the CZA-III samples than for the CZA-I and CZA-II samples. This can be attributed to the difference of the precursor decomposition temperature and decomposition pathways with various La precursors.

Figure 5 displays the adsorption and desorption isotherms of the CZA composite oxides. It can be observed that all samples present mesoporous characteristics. Additionally, there is the presence of hysteresis loops in the isotherms, which are attributed to non-uniform pore shape and size, as well as the phenomenon of capillary condensation. The hysteresis loops of CZA-III are the most prominent regardless of sintering temperature, and the hysteresis loops of CZA-I are less obvious. Hysteresis loop area decreases as a function of increased sintering temperature, especially noticeable for CZA-I. A sharp inflection point related to the rapid uptake of the adsorbate gas is noticed at relative

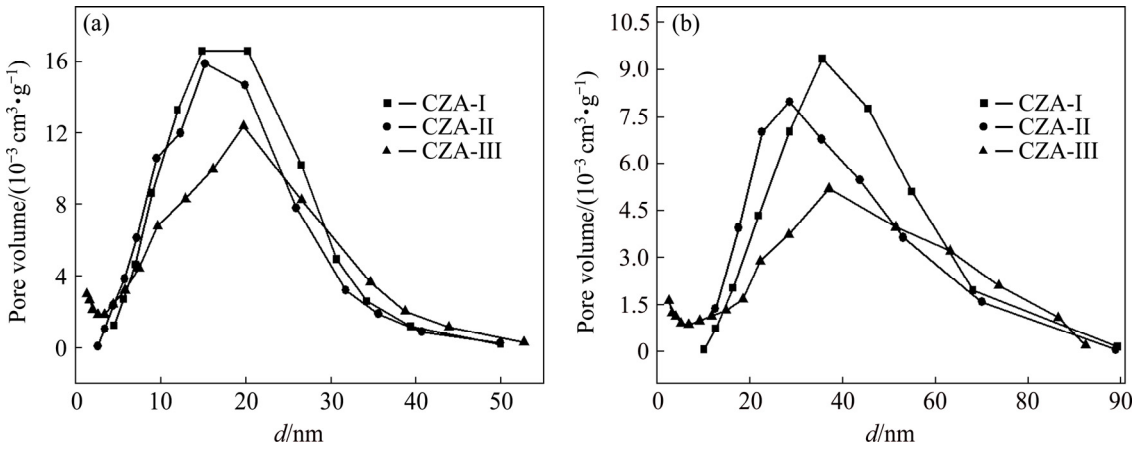

Fig. 4 Pore diameter distributions of CZA samples doped with different La precursors sintered at 1000 °C (a) and 1200 °C (b)

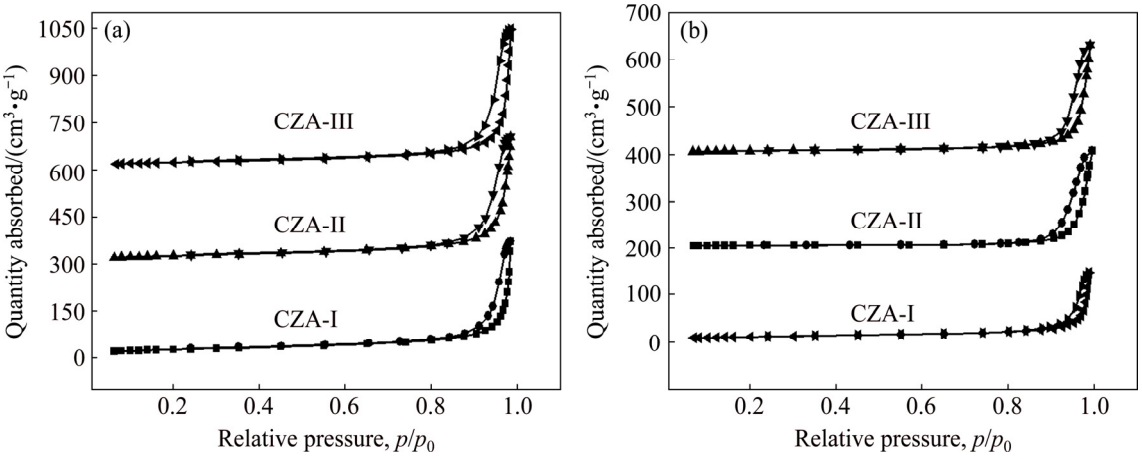

Fig. 5 N_2 adsorption−desorption isotherms of CZA composite oxides doped with different La precursors sintered at 1000 °C (a) and 1200 °C (b)

pressure (p/p_0) of 0.9−1.0, which is related to the mesoporous nature of the interstitial pores.

Usually, the larger the hysteresis loop is, the better the adsorption property is. Hence, the degree of adsorbate uptake is higher for the CZA-III samples, while the adsorption capacity of the CZA-I samples is relatively lower, especially for the samples sintered at 1200 °C.

Textural structure properties and OSC results of the samples are given in Table 1. CZA-III sintered at 1000 °C has the highest surface area (A) with values of 97.46, 72.38 and 40.02 m^2/g at 1000, 1100 and 1200 °C, respectively. While CZA-I has the lowest surface area, the highest mean pore volume and pore diameter regardless of the sintering temperature. On the whole, surface area and pore volume of all samples decrease with the sintering temperature increasing, while pore diameter increases. This can be attributed to either grain growth or crystal transformation resulting in sintering of the interstitial sites or collapsing of the pores at higher temperatures [21,22]. This trend is most obvious for CZA-II, with its specific surface area decreasing by a factor of four, pore volume decreasing by a factor of three, and pore diameter increasing by a factor of three when the sintering temperature is increased from 1000 to 1200 °C. However, the greatest change is within the sintering temperature range of 1100−1200 °C, with a less effect observed when increasing the sintering temperature from 1000 to 1100 °C. This is thought to be related to a dramatic change in the crystalline phase structure of the samples within the sintering temperature range of 1100−1200 °C. There are γ-Al_2O_3 and δ-Al_2O_3 phases in the CZA-I and CZA-II samples sintered at 1100 °C, which do not appear in the CZA-III sample until 1200 °C. This coincides with the XRD analysis results. Hence, the optimum sintering temperature of the CZA oxygen-storage materials is 1100 °C, and the CZA-III sample endures the best anti-high temperature aging performance.

The textural structures of the samples directly affect the oxygen-storage performance. The OSC experiment is performed using a pulse technique, and the results are reported in Table 1. CZA-I samples possess relatively lower OSC values regardless of the sintering temperature,

indicating that OSC efficiency of the CZA oxygen-storage materials is strongly dependent on the specific surface area. CZA-II and CZA-III samples display similar OSC values at 1000 °C, because of their similar textural properties. However, CZA-III samples sintered at 1100 °C show higher OSC values than CZA-I and CZA-II, owing to the enhanced high temperature thermal stability and the oxygen vacancy abundance. It has previously been reported that La^{3+} rare earth ions are dopants that improve OSC and thermal stability of ceria-based oxides, attributed to doping a small amount of La^{3+}, which generates additional oxygen vacancies and crystal defects when La^{3+} is incorporated into the lattice [23,24]. Compared with La_2O_3 and $La(NO_3)_3$, the samples in the presence of the La[EDTA] precursor present higher OSC values, creating more crystal defects, and maintain relatively higher surface areas after high-temperature sintering. The results coincide with the thermal analysis results. From Table 1, we can also observe that the OSC values decline sharply as a function of increased sintering temperature from 1100 to 1200 °C. Specific surface areas decrease by 58.94% and the OSC values decrease by 74.56% when the CZA-III precursor samples are subjected to sintering temperatures from 1100 to 1200 °C. Therefore, the optimum sintering temperature should not exceed 1100 °C.

3.5 TPR analysis

TPR is widely used to characterize the reductive properties of ceria-based materials. Figure 6 displays the H_2-TPR profiles of the CZA composite oxides prepared under different conditions. The composite oxide precursors sintered at 1000 °C exhibit reduction peak values at ~600 °C. CZA-III, employing the La[EDTA] precursor, shows a reduction peak at a maximum value of 635 °C. CZA-II, doped with $La(NO_3)_3$, presents a minimum value of 555 °C, while the corresponding temperature for CZA-I, using La_2O_3 as the precursor, is 570 °C. The reduction peak temperatures of the composite oxides sintered at 1100 °C translate to high temperature zones. The reduction peak temperature for CZA-III, increases by 15 °C to a maximum value of 650 °C. CZA-I presents a reduction peak value of 638 °C, and the reduction peak temperature of CZA-II, synthesized with $La(NO_3)_3$ the precursor, is 618 °C. This is thought to be attributed to the difference in the crystalline phase structure of the samples. The crystalline phase structure of the CZA-III samples does not significantly change at 1000 and 1100 °C; only the crystallinity increases. Meanwhile, minor γ-Al_2O_3 and δ-Al_2O_3 phases are present in the crystalline phases of CZA-I and CZA-II sintered at 1100 °C. However, the crystalline phase structure of all samples show dramatic changes when being subjected to sintering temperature of 1200 °C. The TPR profiles of samples sintered at 1200 °C show either two or even three peaks, which indicates that the reduction mechanism may follow a two- or three-stage process. The peaks present at ~400 °C are related to the reduction of the surface ceria oxide, while bulk reduction is represented by the high-temperature signal at ~650 °C. Furthermore, the $Ce_xZr_{1-x}O_2$ solid solution formation will result in the distortion of the cubic fluorite lattice. As a result, the reduction process is no longer confined to the surface but extended deep into the bulk [16].

Table 1 Textural performance of CZA after sintering with different La precursors

Sample	A/($m^2 \cdot g^{-1}$)			V/($cm^3 \cdot g^{-1}$)			d_p/nm			OSC/(μmol·g^{-1})		
	1000 °C	1100 °C	1200 °C	1000 °C	1100 °C	1200 °C	1000 °C	1100 °C	1200 °C	1000 °C	1100 °C	1200 °C
CZA-I	92.98	62.42	22.14	0.68	0.50	0.24	16.25	25.36	44.05	300.25	256.24	58.47
CZA-II	96.40	69.65	27.69	0.62	0.47	0.25	15.15	23.87	40.23	392.16	285.67	83.54
CZA-III	97.46	72.38	40.02	0.56	0.45	0.22	14.75	20.46	31.51	400.27	312.89	101.81

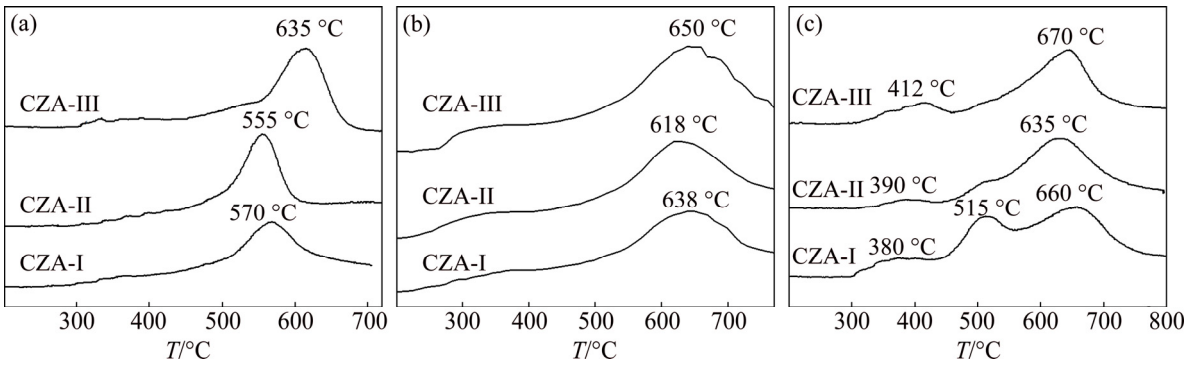

Fig. 6 Temperature-programmed reduction profiles of CZA samples doped with different La precursors after sintering at 1000 °C (a), 1100 °C (b) and 1200 °C (c)

For CZA-III, the reduction temperature is the highest. Doping a small amount of La rare earth ions can enhance specific surface area and promote thermal stability [25]. CZA-III exhibits the highest temperature stability for the five-membered rings composed of metal cations and EDTA, which is consistent with TGA/DSC analysis. For CZA-I, the degree of reduction is the largest at 1200 °C. Reduction capacity of the CZA oxygen-storage materials is associated with their textural structures. Typically, large pore diameters and large pore volumes result in enhanced reduction [26].

4 Conclusions

1) La-doped CZA composite oxides were prepared following a co-precipitation method in the presence of various La precursors, namely, La_2O_3, $La(NO_3)_3·6H_2O$ and $H[La(EDTA)]·16H_2O$. The specific surface area and thermal stability can be enhanced by introducing the $H[La(EDTA)]·16H_2O$ precursor into the solution. Sintering the samples above 1000 °C yields CeO_2−ZrO_2 cubic fluorite as the major phase.

2) The CZA samples that employ $H[La(EDTA)]·16H_2O$ as the precursor display enhanced thermal stability compared with the composite oxides prepared with the La_2O_3 and $La(NO_3)_3·6H_2O$ precursors. The CZA samples possess different porous structure and surface morphologies depending on the La precursor used. Product morphology and pore structure influence the textural properties and OSC of the CZA samples. The samples doped with La_2O_3 show the largest degree of reduction at 1200 °C because of the relatively larger pore volume and pore diameter.

3) The CZA samples sintered at 1000 °C in the presence of the $H[La(EDTA)]·16H_2O$ precursor have the highest surface areas with values of 97.46 m^2/g. The corresponding OSC value is also the largest with value of 400.27 μmol/g when the CZA-III precursor sample is sintered at 1000 °C. From 1100 to 1200 °C, the surface areas and redox properties of the samples decline dramatically. So, the optimum sintering temperatures should not exceed 1100 °C.

References

[1] HECK R M, FARRAUTO R J. Automobile exhaust catalysts [J]. Applied Catalysis A: General, 2001, 221(1−2): 443−457.

[2] KAPAR J, FOMASIERO P, GRAZINI M. Use of CeO_2-based oxides in the three-way catalysis [J]. Catalysis Today, 1999, 50(2): 285−286.

[3] ZHANG Y J, ZHANG L, DENG J G, DAI H X, HE H. Controlled synthesis, characterization, and morphology-dependent reducibility of ceria-zirconia-yttria solid solutions with nanorod-like, microspherical, microbowknot-like, and micro-octahedral shapes [J]. Inorganic Chemistry, 2009, 48(5): 2181−2192.

[4] ZHAO Q S, XIANG J, SUN L S, SHI J M, SU S, HU S. Selective catalytic reduction of NO with NH_3 over sol-gel-derived CuO−CeO_2−MnO_x/γ-Al_2O_3 catalysts [J]. Journal of Central South University Technology, 2009, 16(3): 513−519.

[5] SHYU J Z, WEBER W H, GANDHI H S. Surface characterization of alumina-supported ceria [J]. Journal of Physical Chemistry, 1988, 92(17): 4964−4970.

[6] LI M, LIU Z G, HU Y H, WANG M T, LI H Q. Effect of doping element on catalytic performance of CeO_2−ZrO_2 solid solutions [J]. Journal of Rare Earths, 2008, 36(3): 357−361.

[7] HORI C E, PERMANA H, SIMONG K Y. Thermal stability of oxygen storage properties in a mixed CeO_2−ZrO_2 system [J]. Applied Catalysis B: Environmental, 1998, 16(2): 105−117.

[8] FORNASIERO P, BALDUCCI G, MONTER D. Modification of the redox behavior CeO_2 induced by structural doping with ZrO_2 [J]. Journal of Catalysis, 1996, 164(1): 173−183.

[9] MONTE R D, FORMASIERO P, DESINAN S, KASPAR J. Thermal stabilization of $CexZr_{1-x}O_2$ oxygen storage promoters by addition of Al_2O_3: Effect of thermal aging on textural, structural, and morphological properties [J]. Chemistry Materials, 2004, 16(22): 4273−4285.

[10] BIRGERSSON H, ERIKSSON L, BOUTONNET M, JARAS S G. Thermal gas treatment to regenerate spent automotive three-way exhaust gas catalysts (TWC) [J]. Applied Catalysis B: Environmental, 2004, 54(3): 193−200.

[11] WANG X, GORTE R J, WAGNER J P. Deactivation mechanisms for Pd/ceria during the water-gas-shift reaction [J]. Journal of Catalysis, 2002, 212(3): 225−230.

[12] SI R, ZHANG C H, WANG L M, LI S J, LIN B X, CHU W S, WU Z Y, YAN C H. Enhanced thermal stability and oxygen storage capacity for $Ce_xZr_{1-x}O_2$(x=0.4−0.6) solid solutions by hydrothermally homogenous doping of trivalent rare earths [J]. Journal of Physical Chemistry C, 2007, 111(2): 787−794.

[13] MENG J S, JI Z S. Effect of La_2O_3/CeO_2 particle size on high-temperature oxidation resistance of electrodeposited Ni−La_2O_3/CeO_2 composites [J]. Transactions of Nonferrous Metals Society of China, 2014, 24(11): 3571−3577.

[14] WANG S C, XIE H, LIN Y Y, KENNATH R P, LI T. High thermal stability of La_2O_3 and CeO_2-stabilized tetragonal ZrO_2 [J]. Inorganic Chemistry, 2016, 55(5): 2413−2420.

[15] BOZO C, GUIHAUME N, HERRMANN J M. Role of the ceria–zirconia support in the reactivity of platinum and palladium catalysts for methane total oxidation under lean conditions [J]. Journal of Catalysis, 2001, 203(2): 393−406.

[16] WANG L J, WANG K C, CAO H Y, CHEN Y D, LIU Z M. Low temperature catalytic combustion of cooking fume over Pt/γ-Al_2O_3/$CexZr_{1-x}O_2$ catalyst [J]. Acta Physico-Chimica Sinica, 2009, 24(4): 689−693.

[17] LI M, LIU Z G, HU Y H, WANG M T, LI H Q. Effect of doping elements on catalytic performance of CeO_2−ZrO_2 solid solutions [J]. Journal of Rare Earths, 2008, 26(3): 357−361.

[18] WANG S J, XU Y B, LU P X, XU C F, CAO W. Synthesis of yttrium aluminum garnet(YAG) from an ethylenediaminetetraacetic acid precursor [J]. Materials Science and Engineering B, 2006, 127(2−3): 203−206.

[19] FAN J, WENG D, WU X D, WU X D, RAN R. Modification of CeO_2−ZrO_2 mixed oxides by coprecipitated/impregnated Sr: Effects on the microstructure and oxygen storage capacity [J]. Journal of Catalysis, 2008, 258(1): 177−186.

[20] FAN J, WU X D, WU X D, LIANG Q, RAN R, WENG D. Thermal ageing of Pt on low-surface-area CeO_2−ZrO_2−La_2O_3 mixed oxides: Effect on the OSC performance [J]. Applied Catalysis B: Environmental, 2008, 81(1−2): 38−48.

[21] ANG M L, OEMAR U, SAW E T, MO L, KATHIRASE R Y, CHIA B H, KAWI S. Highly active Ni/xNa/CeO_2 catalyst for the water-gas shift reaction: Effect of sodium on methane suppression [J]. ACS Catalysis, 2014, 4(9): 3237−3248.

[22] WANG J, WEN J, SHEN M Q. Effect of interaction $Ce_{0.7}Zr_{0.3}O_2$ and Al_2O_3 on structure characteristics, thermal stability and oxygen storage capacity [J]. Journal of Physical and Chemistry, 2008, 112(13): 5113−5122.

[23] LEMONIDOU A A, VAGIA E C, LERCHER J A. Acetic acid reforming over Rh supported on La_2O_3/CeO_2–ZrO_2: Catalytic performance and reaction pathway analysis [J]. ACS Catalysis, 2013, 3(9): 1919−1928.

[24] JIANG P, LU G, GUO Y, WANG X. Preparation of La_2O_3-doped CeO_2−ZrO_2 solid solution with high thermal stability by water-in-oil microemulsion [J]. Chemistry Letters, 2004, 33(8): 1064−1065.

[25] KONDAKINDI R R, THALLADA B, KOMANDUR V R C. Structure and reactivity of molybdenum oxide catalysts supported on La_2O_3-stabilized tetragonal ZrO_2 [J]. Langmuir, 2003, 19(26): 10795−10802.

[26] KASPAR J, FORNASIERO P, HICKEY N. Automotive catalytic converters: Current status and some perspectives [J]. Catalysis Today, 2003, 77(4): 419−449.

不同 La 源对 CeO_2−ZrO_2−Al_2O_3 复合氧化物结构和性能的影响

李友凤[1]，贺跃辉[2]，刘国清[1]，曾令玮[1]

1. 湖南科技大学 化学化工学院，湘潭 411201；
2. 中南大学 粉末冶金研究院，长沙 410083

摘　要：分别以 La_2O_3、$La(NO_3)_3·6H_2O$ 和 $H[La(EDTA)]·16H_2O$ 为 La 源，采用共沉淀法制备 La 掺杂 CeO_2−ZrO_2−Al_2O_3 复合氧化物样品，即 CZA-I、CZA-II 和 CZA-III，研究不同 La 源对材料结构和性能的影响。结果表明，前躯体沉淀经 1000 °C 煅烧后样品主要为 CeO_2−ZrO_2 相；煅烧温度为 1100 °C 和 1200 °C 时，发现存在 γ-Al_2O_3 与 δ-Al_2O_3 相。高温热处理后，CZA-III 具有比 CZA-I 和 CZA-II 更好的热稳定性。N_2 吸附−脱附结果显示，CZA-III 具有最大的比表面积，其前躯体经 1000 °C 煅烧后所得样品的比表面积值为 97.46 m^2/g，且相应的储氧能力(OSC)值也最大，其值为 400.27 μmol/g，这导致 CZA-III 具有最好的热稳定性和最高的还原温度。然而，当煅烧温度从 1100 升高到 1200 °C 时，复合氧化物样品的比表面积和储氧性能急剧下降，CZA-III 的比表面积值降低 58.94%，OSC 值降低 74.56%。

关键词：La 源；铈锆固溶体；复合氧化物；织构特性；氧化还原性能

(Edited by Bing YANG)